Indian Journal of Pure & Applied Physics
Vol. 57, October 2019, pp. 709-712

Effect of growth temperature and RF power on structural and optical properties of sputtered deposited PbS thin films

Jyotshana Gaur, Hitesh Kumar Sharma, Sanjeev K Sharma & Beer Pal Singh*

Department of Physics, CCS University, Meerut 250 004, India

Received 22 May 2019; accepted 08 July 2019

Lead sulphide (PbS) nanocrystalline thin films have been grown from sputtering with the variation of growth temperature and RF-Power. The intensity of single dominant peak (200) in XRD-pattern increases by increasing the growth temperature from 175 ^{o}C to 200 ^{o}C and RF power from 80 W to 100 W, respectively. The crystallite size and the strain of as-deposited PbS thin films have been calculated from XRD-peak profile analysis. Microscopic surface and cross-section images show the improvement in thin films growth in terms of alignment of grains and thickness. The band gap of PbS thin films has been determined from UV-Vis absorption spectra, where the band gap decreases from 1.98 eV to 1.72 eV as the growth temperature and power increased from 175 °C and 80 W to 200 °C and 100 W.

Keywords: PbS thin films, Growth temperature and RF-power, Structural, Optical properties

1 Introduction

Recently, lead sulphide (PbS) has attracted considerable attention due to its morphological, optical and opto-electronic properties for the application of optoelectronic devices, photoconductors, sensors and infrared detectors[1-3]. The PbS is a IV-VI direct band gap versatile semiconductor material and a large exciton Bohr radius of 18 nm resulting in a high degree of spectral tenability from 3000 nm to visible wavelengths [4-6].

Nanocrystalline PbS thin films have been deposited on conducting and non-conducting substrates for various optoelectronic devices [6,7]. PbS thin films can be deposited by different chemical and physical methods, such as vacuum evaporation[2,8], successive ionic layer adsorption and reaction (SILAR)[9], electro-deposition[10,11], chemical bath deposition (CBD)[12], RF-sputtering[1,13-16] and so on. Among these deposition methods, the RF-sputtering is one of the precise methods to deposit PbS thin films, which can control the deposition rate and microstructure by manipulating the optimised growth temperature to avoid environmental contaminations and defects[13, 14].

Despite the extensive study of PbS thin films for various applications, there are fewer studies for the growth of PbS thin films by controlling the temperature and power simultaneously. Therefore, the microstructure, structural and optical properties of sputtered deposited PbS thin films with optimised process parameters are studied for the future prospective applications.

2 Experimental

PbS thin films were deposited on glass substrates by RF sputtering at the growth temperature of 175 ^{o}C and 200 ^{o}C with RF-power of 80 W and 100 W, respectively. Prior to the deposition of PbS thin films, the substrate was cleaned by acetone, methanol and DI water and dried by compressed nitrogen gas for 10 min at room temperature. For the source of PbS, the target was purchased from commercially available "Advanced Process Technology" with a high purity of 99.9%. This PbS target was loaded in the sputtering system for deposition of PbS thin films. The argon gas (Ar) was used to produce plasma with the flow rate of 20.1 sccm. During the PbS thin films growth, the pressure was maintained in the chamber to be ~ 2.4×10^{-2} mbar. For the optimization of PbS thin films, two growth parameters, that is, the RF-power and the growth temperature were varied. For all grown samples, the deposition time was fixed for 30 min. The prepared PbS thin films were characterized by using different analysis tools. The diffraction patterns of PbS thin films were measured by X-ray diffractometer (XRD) by using $CuK_{\alpha 1}$ radiation (0.154056 nm) X-ray source operating at 40 kV and

*Corresponding Author: (E-mail: drbeerpal@gmail.com)

40 mA, at a Bragg-Brentano θ-2θ configuration, with an incidence of 1° (Rigaku-Ultima-IVsystem, Japan). The structural parameters (the crystallite size, and strain) were calculated from XRD-peak profile analysis. The surface and cross-sectional microstructure of thin films were determined from field emission scanning electron microscopy (FE-SEM)(Hitachi-S-4700). The elemental composition of PbS thin films was measured by EDAX spectra. The optical properties of films (band gap, nature of band gap) were determined from UV-Vis spectrophotometer (US-S-4100) referenced to an air. The band gap was calculated from the Tauc's plot.

3 Results and Discussion

Figure 1 (a – c) show the XRD patterns of PbS thin films grown at three different conditions, that is, 80 W and 175 °C, 80 W and 200 °C, and 100 W and 200 °C, respectively. The preferred and dominant peak (200) of films was observed at 30° (2θ) in all samples regardless of growth conditions. While the peak intensity increased with respect to increasing the RF-power from 80 W to 100 W and the growth temperature from 175 °C to 200 °C. At the growth conditions of 100 W and 200 °C (Fig. 1 (c)), the diffusion of sputtered species increased, and allowing them to deposition site on the substrate to form uniform and align the crystals[13]. The second diffraction peak was also appeared at 62° corresponding to the (400) plane. Both peaks (200) and (400) of PbS thin films are confirmed by standard data of JCPDS card no. 5-0592. The crystallite size (D) was calculated through the Debye-Scherrer's formula[17]:

$$D=0.9\lambda/\beta\cos\theta \quad \ldots(1)$$

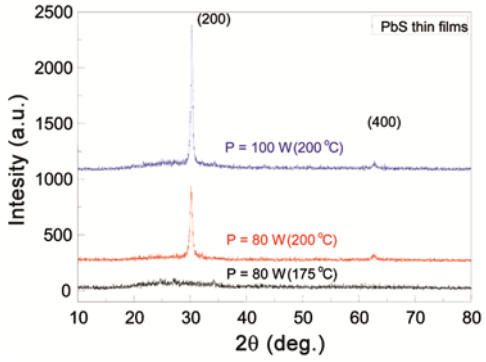

Fig. 1 – XRD-pattern of PbS thin films with respect to the variation of RF-power (P) and temperature (T), (a) P = 80 W, T = 175 °C, (b) P = 80 W, T = 200 °C and (c) P = 100 W, T = 200 °C.

where, λ is the wavelength of X-ray of Cu-K_α (0.154056 nm) and β is the FWHM of a diffraction peak centered at an angle θ. The strain was calculated with the help of following formula[18]:

$$\varepsilon=\beta/4\tan\theta \quad \ldots(2)$$

where, β is the FWHM of a diffraction peak centered at an angle θ. Figure 2 shows the variation of FWHM, crystallite size, and the strain of PbS thin films. The crystallite size of PbS thin films was increased from 13 to 17 nm as the growth parameters were changed from 80 W and 175 °C to 100 W and 200 °C, respectively. While, the strain of PbS thin films was decreased from 10.5 to 7.4 by changing the growth parameters from 80 W and 175 °C to 100 W and 200 °C, respectively. The increasing crystallite size and decreasing the strain in thin films might be occurred due to the improvement in alignment and uniform the growth crystals.

Figure 3 (a -f) shows the surface and the respective cross-section microstructures of PbS thin films grown at 80 W and 175 °C, 80 W and 200 °C, and 100 W and 200 °C, respectively. The grain size was also calculated by using the surface scale mapping from microscopic SEM images.

The average grain size of PbS films decreased from 200 to 120 nm as the growth temperature and power increased from at 175 °C and 80 W to 200 °C and 100 W. The average thickness of PbS thin film decreased from 300 nm to 250 nm as the growth temperature increased 175 °C to 200 °C, while keeping the RF power of 80 W. Thereafter, the average thickness of PbS thin films increased from 250 nm to 320 nm as the RF power increased from 80 W to 100 W and kept constant the growth temperature of 200 °C. Increasing the film thickness and decreasing the grain size of

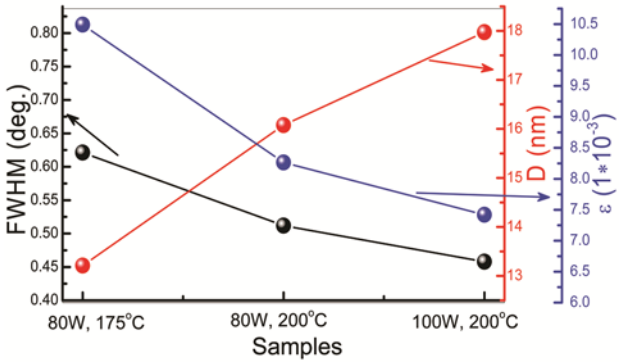

Fig. 2 – Structural parameters determined from XRD-peak profile analysis, FWHM, crystallite size (D) and strain (ε).

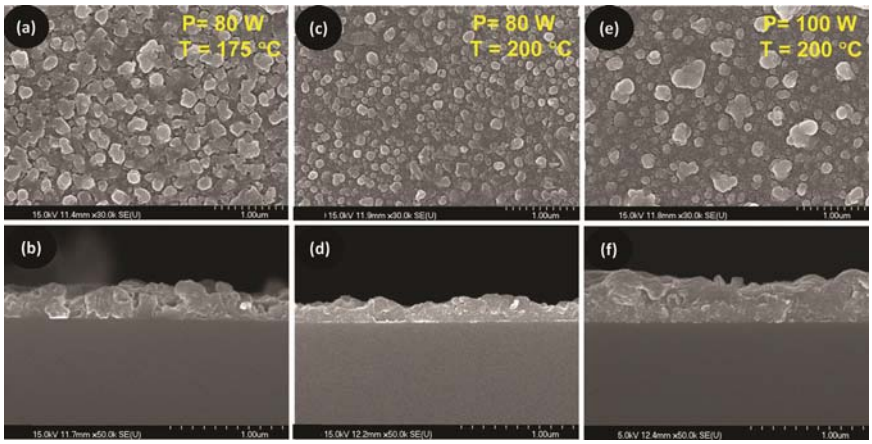

Fig. 3 – FE-SEM microscopic images of PbS thin films, (a) and (b) surface and cross-section at P = 80 W, T = 175 °C, (c) and (d) surface and cross-section at P = 80 W, T = 200 °C, (e) and (f) surface and cross-section at P = 100 W, T = 200 °C.

PbS thin films by increasing the RF power from 80 W to 100 W and the growth temperature from 175 °C to 200 °C could be occurred due to growth rate increased by increasing the RF power and growth temperature. Some of grains are agglomerated on the surface microstructure that is clearly reflected from the images due to the highest growth rate. To determine the chemical composition and the stoichiometric of PbS thin films, the EDAX spectrum was measured at room temperature. Figure 4 shows the typical EDAX spectrum of PbS thin films of the sample grown at the highest RF power of 100 W and the highest growth temperature of 200 °C. Strong peaks of Pb and S were observed in the spectrum. The absence of other sharp peaks in the spectrum is confirmed the formation of PbS stoichiometry of films. While some of the lower intensity peaks were also detected, that were not related to the sample. For the typical as-deposited sample at 200 °C and 100 W, the stoichiometry ratio (at.%) of Pb and S, that is, Pb:S=39:61 was achieved.

The optical band gap of the sputtered PbS thin films was determined from Tauc's plot by the extrapolation of linear portion of the $(\alpha hv)^2$ versus the photon energy (hv) as shown in Fig. 5. The Tauc's relation was used as given below[19, 20]:

$$\alpha hv = A(hv - E_g)^n \quad ...(3)$$

where, α is the absorption coefficient, hv is the energy of incident photons, E_g is the optical band gap and A is the proportionality constant and n =1/2 for direct band gap materials[21].

$$(\alpha hv)^2 = A(hv - E_g) \quad ...(4)$$

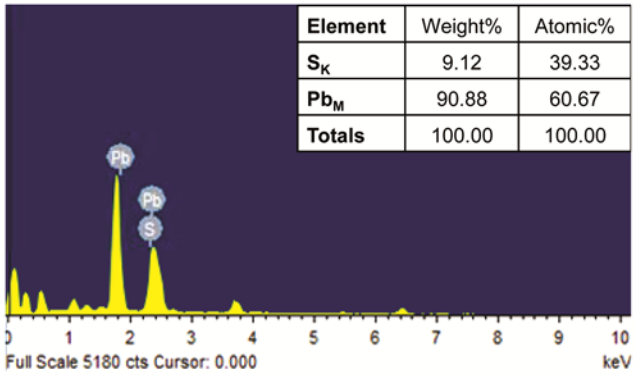

Fig. 4 – Typical EDAX spectrum of PbS thin film deposited at 200 °C by applying RF power of 100 W.

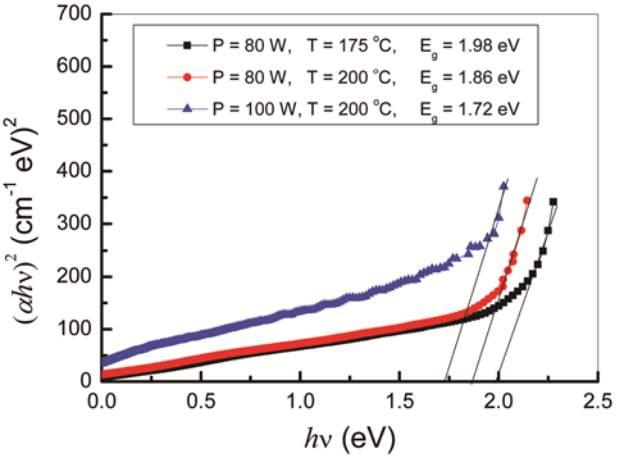

Fig. 5 – Tauc's plot for the determination of bandgap for PbS thin films grown by RF-sputtering with the variation of RF-power and growth temperature.

The band gap of as-deposited sputtered PbS thin films was decreased from 1.98 to 1.72 eV by increasing the RF power and growth temperature from 80 W and 175 °C to 100 W and 200 °C. The

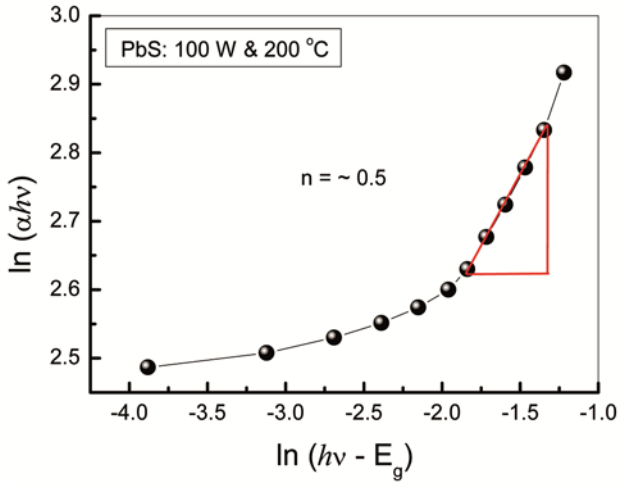

Fig. 6 – Plot of ln(α$h\nu$]) versus ln($h\nu - E$g) of as-grown sputtered PbS thin film (power = 100 W and growth temperature = 200 °C). The slope (n) ~0.5 shows the direct type transition.

increasing band gap of sputtered PbS thin films with increasing the growth temperature and power was occurred due to the effect of quantum confinement[22]. The nature of the optical band gap of the as-deposited sputtered PbS thin films was studied by using logarithm form of Tauc's equation as follows[23]:

$$\ln(\alpha h\nu) = \ln A + n\ln(h\nu - E_g) \quad ...(5)$$

The value of the optical band gap (E_g) of the as-deposited sputtered PbS thin films was used to study the nature of the band gap. The significance of nature of band gap is to analyze the feasibility of the material for the application of optoelectronic devices. The slope of linear region of the plot ln($\alpha h\nu$) versus ln($h\nu - E_g$) is shown in Fig. 6. The value of "n =1/2" is indicated an allowed direct transition in the as-deposited sputtered PbS thin films.

4 Conclusions

Nanocrystalline PbS thin films were grown on glass substrates by RF-sputtering with the controlling growth temperature and RF-power. The crystalline behaviour of sputtered PbS thin films improved with respect to increasing the growth temperature from 175 °C to 200 °C and RF power from 80 W to 100 W. The average grain size of PbS films decreased from 200-120 nm as the growth temperature and power increased from at 80 W and 175 °C to 100 W and 200 °C. The band gap of PbS thin films decreased from 1.98 to 1.72 eV as the power and temperature increased from 80 W and 175 °C to 100 W and 200 °C.

Acknowledgement

The funding for this research work was supported from DST-FIST sponsored project SR/FST/PSI-177/2012. One of the authors Ms. Jyotshana Gaur, was partially supported from the CCS University under the student scholarship program.

References

1 Motlagh Z A & Araghi M E A, *Mater Sci Semicond Process*, 40 (2015) 701.
2 Abhilash A, Nair A S, Rajasree S, Hiba R E & Pradeep B, *AIP Conf Proc*, 1665 (2015) 080024.
3 Perera A G U, Jayaweera P V V, Ariyawansa G, Matsik S G, Tennakone K, Buchanan M, Liu H C, Su X H & Bhattacharya P, *Microelectr J*, 40 (2009) 507.
4 Sarica E & Bilgin V, *Mater Sci Semiconduct Process*, 71 (2017) 42.
5 Yücel E, Yücel Y & Beleli B, *J Alloys Compd*, 642 (2015) 63.
6 Xu J, Sutherland B R, Hoogland S, Fan F, Kinge S & Sargent E H, *Appl Phys Lett*, 107 (2015) 153105.
7 Hone F G & Dejene F B, *J Lumin*, 201 (2018) 321.
8 Singh B P, Kumar R, Kumar A & Tyagi R C, *Mater Res Exp*, 2 (2015) 106401.
9 Güneri E, Göde F & Çevik S, *Thin Solid Films*, 589 (2015) 578.
10 Saloniemi H, Kemell M, Ritala M & Leskelä M, *Thin Solid Films*, 386 (2001) 32.
11 Aghassi A, Jafarian M, Danaee I, Gobal F & Mahjani M G, *J Electroanal Chem*, 661 (2011) 265.
12 Yücel E & Yücel Y, *Ceram Int*, 43 (2017) 407.
13 Filho J M C S & Marques F C, *Mater Sci Semiconduct Process*, 91 (2019) 188.
14 Solis-Pomar F, Cruz A F, Menchaca J L, Meléndrez M F & Pérez-Tijerina E, *Mater Res Exp*, 5 (2018) 106403.
15 Filho J M C S, Ermakov V A & Marques F C, *Sci Rep*, 8 (2018) 1563.
16 Nasu H, Yamada H, Matsuoka J & Kamiya K, *J Non-Crystalline Solids*, 183 (1995) 290.
17 Sharma S K & Kim D Y, *J Mater Sci Technol*, 32 (2016) 12.
18 Kumar R, Das R, Gupta M & Ganesan V, *Superlatt Microstruct*, 75 (2014) 601.
19 Sharma S K, Baveja J & Mehra R M, *Phys Status Solidi A*, 194 (2002) 216.
20 Kaur N, Sharma S K, Kim D Y & Singh N, *Physica B: Condensed Matter*, 500 (2016) 179.
21 Suwanboon S, Amornpitoksuk P, Haidoux A & Tedenac J C, *J Alloys Compd*, 462 (2008) 335.
22 Rajathi S, Kirubavathi K & Selvaraju K, *Arab J Chem*, 10 (2017) 1167.
23 Singh B P, Upadhyay R K, Kumar R, Yadav K & Areizaga-Martinez H I, *Adv Opt Technol*, 2016 (2016) 6.